

Chapter 9

Modelling the creep rupture life of austenitic stainless steels

Being able to predict quantitatively the creep rupture life of a steel, or its 10^5 h creep strength is of enormous interest for the design of alloys and their use in the power generation industry. Although tests cannot be avoided, a good quantitative model allows a considerable reduction in the number of trials needed to match the expected properties.

When complex properties such as creep life or toughness are addressed, physical models are mostly of qualitative use, but are yet not able to deliver accurate quantitative predictions as a function of the large number of controlling variables. Such problems have long been solved using empirical modelling and experience. Most widely used are probably the multi-linear and polynomial regressions (for example, in NRIM datasheet 6B, the tensile strength is modelled using a 3rd order polynomial). The methods have some advantages: they require a small number of coefficients and are generally simple to calculate. On the other hand, their flexibility is limited. They do not allow sufficient interactions between the different input variables and consequently their range of validity may be narrow. However, the continuous increase in computing power allows much more complex regression methods to be implemented relatively easily.

9.1 Neural Networks for empirical modelling

All regression methods can be described generally in terms of neural networks. To define a neural network, it is first necessary to present the single neuron.

9.1.a The single neuron

A single neuron has a given number of inputs x_i , and an output y . A weight w_i is associated with each input. The activation a of the neuron is defined by:

$$a = \sum_i w_i x_i \quad (9.1)$$

Equation 9.1 sometimes takes the form $\sum_i (w_i x_i + h)$, where h is called the bias, but in practice, this additional term is included in the general notation by considering w_0 associated with the constant input 1.

A single neuron output is a function of its activation $y(a) = f(a)$, where the function f depends on the problem considered.

9.1.b More complex networks

The standard feedforward networks used in this work consist of 2 layers of neurons interconnected as described in figure 9.1. These networks are also referred to as three layers network which are the inputs, the hidden units and the output. The second layer

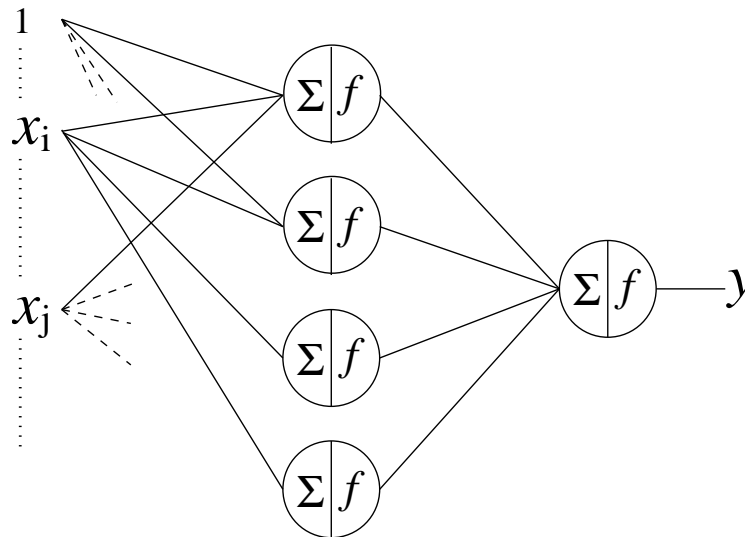


Figure 9.1: A three layers feedforward network identical to the one used in this work. The activation function of the neurons in the first layer is a tanh, and is linear in the second one. The complexity of the model is controlled by the number of hidden units.

is often referred to as ‘hidden layer’ and its neurons as hidden units. Their activation

function is non-linear, in the present case a tanh function. The third layer performs a linear combination of each hidden unit output.

9.1.c Neural Network as a regression tool

In supervised learning, the network is presented with a data set $D = \{\mathbf{x}^{(n)}, \mathbf{t}^{(n)}\}$, and the weights are adjusted so as to minimise an error function. In the light of the description of a single neuron, performing a linear regression on a data set D can be described as training a single neuron with a linear activation function. In the case of the two layer network in figure 9.1, the learning process is equivalent to a multiple, non-linear regression. The existence of an intermediate layer also allows the model to identify interactions between variables.

9.1.d Learning and making predictions

The algorithm used to train the models has been written by D.J.C. Mackay. It implements a particular learning method using Bayesian statistics to infer the most probable distribution for the weights given the data.

i A simple example of inference

A good example to illustrate Bayes rule is that of someone drawing balls from 11 urns each containing 10 balls. Of the 10 balls in each urn, u are black, and the rest are white. Given that the person draws N times (replacing the balls on each occasion) from a chosen

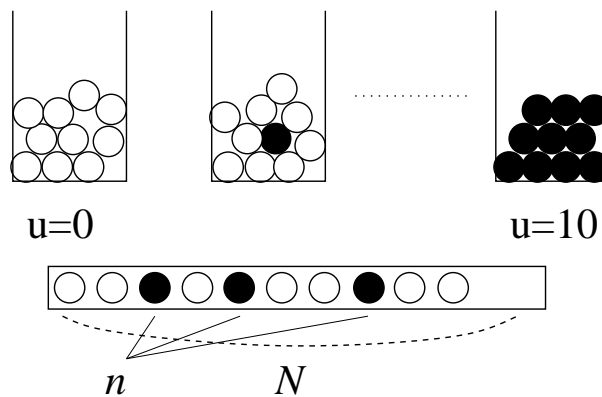


Figure 9.2: A person is drawing N times from a same urn u chosen among ten and presents the result. The problem is to guess which urn the person has chosen and to use this to predict the next draw.

urn, the problem is to guess from which urn u the person has drawn. In this case, Bayes

rules is written:

$$P(u|n, N) = \frac{P(n|u, N) P(u|N)}{P(n|N)} \quad (9.2)$$

that is, given that the person has drawn n black balls among N , the probability that urn u was used is the probability of drawing n black balls from u times the probability to chose u , over the overall probability of drawing n balls. This last term is also:

$$P(n|N) = \sum_u P(n|u, N) P(u|N) \quad (9.3)$$

To solve the problem, we can first assume (this is our hypothesis H) that the person will chose any of the urns with the same probability, so that $P(u|N)$, which is actually $P(u)$ since it does not depend on the number of draws, is $1/11$; this is called the *prior*. For each possible value of u , we can then compute the probability of drawing n black balls, which gives a binomial distribution. If we are simply interested in knowing which urn the person has most probably drawn from, that is to compare the different models, there is no need to calculate the normalising constant $P(n|N)$. The result is a probability distribution on u , which, not surprisingly, is maximum for $n = u$. However, almost all other possibilities have a non zero probability, as can be seen in figure 9.3, apart from the two urns containing either only white or only black balls.

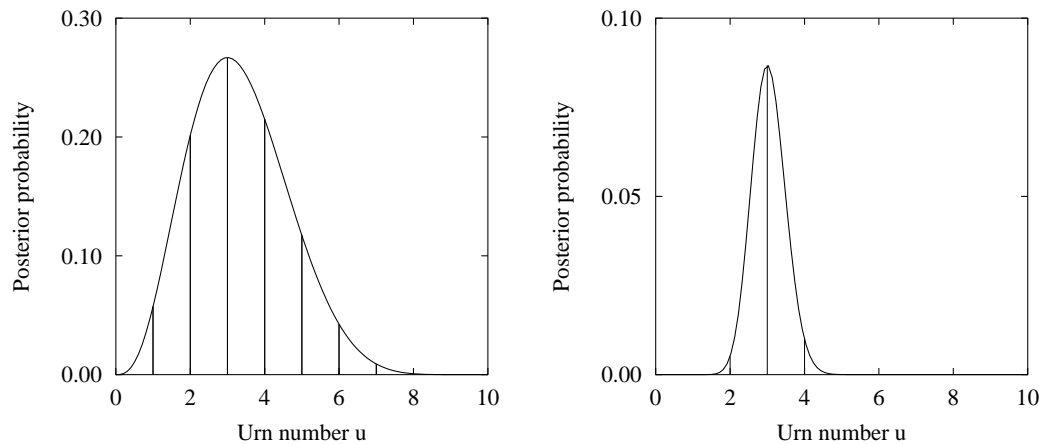


Figure 9.3: The posterior probability for the chosen urn u , when $n = 3$ ($N = 10$). The person has most probably drawn from the urn containing 3 black balls, but the probability that he/she has drawn from other urns is not negligible. The right figure shows that when more data are presented, ($n = 30$, $N = 100$) the probability of $u = 3$ is much greater than $u = 2$ and $u = 4$ and that any other value of u is virtually impossible

An interesting problem is to now use these results to predict how likely the person is to obtain a black ball at the next draw. For this, we consider the different possible values of u with their respective probability; for each of them, the probability of obtaining a black ball is $u/10$, so the overall probability is

$$\sum_{u=1}^{u=10} P(u|n, N) u/10 \quad (9.4)$$

This process is called *marginalizing* over all the possible values of u .

A traditional statistic approach would have used the most probable hypothesis ($u = 3$) to make this prediction, and would have led to a value of $1/3$. In the Bayesian approach, all the possibilities are taken into account, but weighted according to how probable they are.

ii Quantifying the uncertainty

One of the most interesting features of the Bayesian approach to inference problems, is that it provides a quantitative estimation of the uncertainty in fitting a model to the data. Figure 9.3 shows the posterior distributions for $P(u)$ when $n = 3$, $N = 10$ and $n = 30$, $N = 100$. In the first case, the distribution is spread, while it is sharply peaked in the second one. Consequently, the predictions made on the basis of the second model ($n = 30$, $N = 100$) is associated with a much smaller uncertainty than those made using the first set of data. The reader interested in the relatively complex mathematical treatment of this problem can refer to [110].

iii Application to neural network learning

Neural networks are usually trained by minimising an error function such as equation 9.5:

$$\begin{aligned} M(\mathbf{w}) &= \beta E_D + \alpha E_W & (9.5) \\ E_D &= \frac{1}{2} \sum_i (t^{(i)} - y^{(i)})^2 \\ E_W &= \frac{1}{2} \sum_i w_i^2 \end{aligned}$$

where E_D is the overall error, and E_W the regulariser, used to force the network to use small weights (equations 9.5). α and β are control parameters which largely influence

the complexity of the model. $t^{(i)}$ is the target for the set of inputs $\mathbf{x}^{(i)}$, while $y^{(i)}$ is the corresponding network output.

The method used in this study, developed by MacKay [111], is based on Bayesian probability theory and treats learning as an inference problem.

Rather than trying to identify the best set of weights, the algorithm infers a probability distribution for the weights from the data presented. When making predictions, the variety of solutions corresponding to different possible sets of weights are averaged using the probabilities of these sets of weights, a process called *marginalising*.

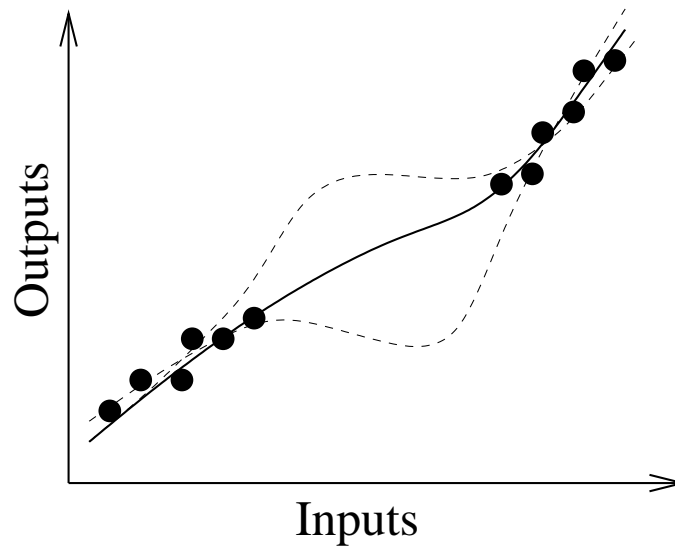


Figure 9.4: Where data are sparse, the probability distribution of the weights is wider, and predictions are accompanied by a larger error bar.

A major consequence is that it is possible to quantify the uncertainty of fitting: if the inferred distribution is sharply peaked in the weight space, the most probable set will give by far the largest contribution to the prediction and alternative solutions will have little importance. As a consequence, the prediction will be associated with a small uncertainty. If on the contrary, the data are such that different sets of weights are similarly probable, alternatives will contribute in similar proportions and the error bar will be large, as typically occurs in regions of the input space where data are scarce or exceptionally noisy. This is illustrated in figure 9.4.

In this context, the performances of different models are best evaluated using the log predictive error (LPE) as defined below. This error penalises wild predictions to a lesser

extent when they are accompanied by appropriately large error bars.

$$\text{LPE} = \sum_m \left[\frac{1}{2} (t^{(m)} - y^{(m)})^2 / \sigma_y^{(m)2} + \log \left(\sqrt{2\pi} \sigma_y^{(m)} \right) \right] \quad (9.6)$$

where $\sigma_y^{(m)}$ is related to the uncertainty of fitting for the set of inputs $\mathbf{x}^{(m)}$.

9.1.e Practical aspects of the neural network training

i The overfitting problem

Because of the great flexibility of the functions used in the network, there is a possibility of overfitting data. Two solutions are implemented which contribute to avoid overfitting. The first is contained in the algorithm due to MacKay: the complexity parameters α and β are inferred from the data, therefore allowing automatic control of the model complexity.

The second resides in the training method. The database is equally divided into a training set and a testing set. To build a model, about 150 networks are trained with different numbers of hidden units and seeds, using the training set; they are then used to make predictions on the unseen testing set and are ranked by LPE. Figure 9.5

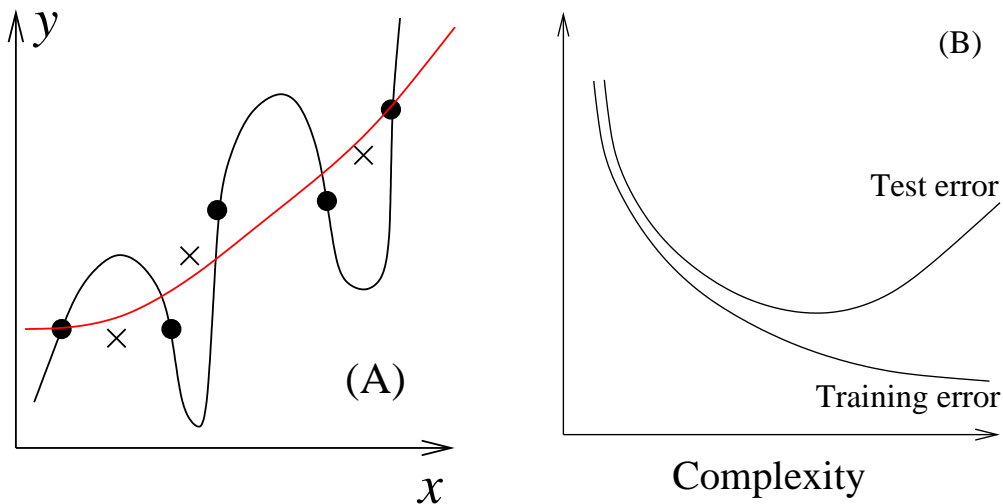


Figure 9.5: (A) When a model has overfitted the training data (\bullet), the error on the test data (\times) is larger than for an optimum model which fits the trend but not the noise. (B) illustrates the behaviour of the error on the training and testing sets as a function of the complexity of the model.

illustrates the behaviour of the error on the training and the testing set. Because it is

possible to obtain a near perfect fitting, the error on the training set is always decreasing with increasing complexity. The error on the testing set decreases at first, as the fitting improves, but increases again when overfitting occurs.

ii Choice of variables

Careful selection of the input variables and of the output is essential to the construction of a good model. For example, if a particular combination of two variables is thought to be of particular importance, it can be included as a variable itself. The same applies to functions of relevant variables. In creep problems for example, $\log(t)$ is much more relevant than t , and models trained to predict $\log(t)$ perform much better than those with t as an output.

Because the algorithm includes an automatic relevance detection [110], variables which are either redundant or found to be irrelevant are affected a zero weight. There is therefore little to gain in reducing the number of input variables by any other process.

iii Other practical aspects of the training

To ensure a good distribution of the data in the data set, it is first randomised, or rather re-organised, with every odd line being moved to the testing set. However, this procedure has been found to be inappropriate in this particular case, as will be explained later. Another important step is the normalisation, which brings the range of variations of all the variables between -0.5 and 0.5 . This is to avoid having very different scales of variations between the different inputs.

9.1.f Committee Model

The complexity of a model depends on its number of hidden units. Therefore, models with different numbers of hidden units will give different predictions.

To explain the origin of another potential difference between models, the example of the urn is useful. To estimate the probability of a black ball being drawn at $N + 1$, it was first assumed that the choice of the urn was totally random, ie $P(u) = u/11$. However, this might not be the case. Maybe some are easier to access than others? For example, if urn 4 is much easier to access than urn 3, our final guess of which urn has most probably been used might be changed, particularly if N is relatively small, as in figure 9.3 where 3 and 4 are not far from equiprobable under the assumption $P(u) = 1/11$.

This illustrates the fact that the *prior* $P(u)$ or $P(\Theta|H)$ in the general case, is important

for our predictions.

The same apply when calculating the posterior distribution $P(\mathbf{w}|\alpha, \beta, H)$. For a given number of hidden units, the predictions of a model still depends more or less strongly on the prior distribution of the weights. In practice, the distribution is assumed to be a Gaussian, whose parameters are fixed by a seed.

i The training process

For this reason, the training process involves in fact the training of a large number of models with different numbers of hidden units (typically 1 to 25), and different priors, that is different seeds (typically 5).

These models are then ranked according to how they perform on unseen data. Most of the time, a combination of the best models performs better than a single model.

ii Committee model

To determine the optimum number of models to use in a committee, the combined prediction error is calculated for an increasingly large number of models. Most of the time, this combined error presents a minimum which corresponds to the optimum number of models to be used (see figure 9.6). The committee prediction is the average of

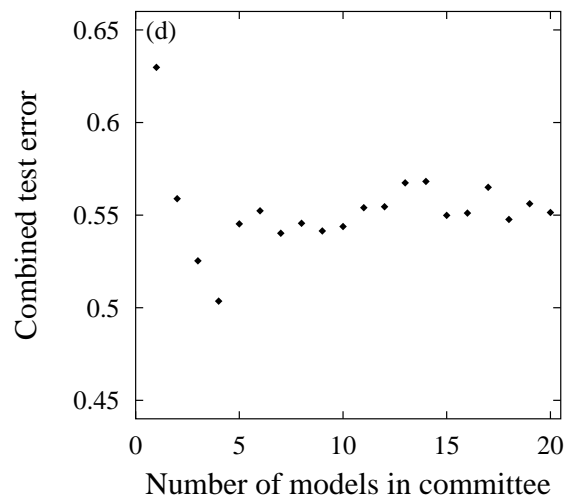


Figure 9.6: An example of the variation of the combined test error when the number of model in the committee is increased. In this case, the optimum number of model is found to be 4

the predictions of the models constituting the committee, while the error is calculated

according to:

$$\begin{aligned}\bar{y} &= \frac{1}{L} \sum_l y^{(l)} \\ \sigma^2 &= \frac{1}{L} \sum_l \sigma_y^{(l)2} + \frac{1}{L} \sum_l (y^{(l)} - \bar{y})^2\end{aligned}\quad (9.7)$$

where L is the number of networks in the committee, and, in this particular case, σ is the standard deviation. Note that we now consider the predictions for a given, single set of inputs and that the exponent (l) refers to the model used to produce the corresponding prediction $y^{(l)}$. In practice, an increasing number of networks are included in a committee and their performances are compared on the testing set. Most often, the error is minimum when the committee contains more than one model. The selected models are then retrained on the full database.

9.2 Traditional empirical method for creep strength predictions

The need for quantitative predictions of the creep strength, or the rupture life, of austenitic stainless steels has led to the use of more or less complex regression methods.

For example, the influence of some alloying elements has been studied [6] using linear regression, such as equation 9.8 or 9.9, which estimate the 10^4 h creep rupture stress as a function of the composition in wt%, for AISI 316 and 304 respectively.

$$\sigma_{f,10^4\text{h}} = 173.8 + 7243(\text{B}) + 961.1(\text{N}) + 1145(\text{S}) - 7.5(\text{Cr}) \quad (9.8)$$

$$\sigma_{f,10^4\text{h}} = 90.81 + 115(\text{Mo}) + 498.5(\text{W}) \quad (9.9)$$

The NRIM (National Research Institute for Metals, Japan) uses traditional methods to fit the creep curves of each steel studied. Typically, a time-temperature parameter such as the one given in equation 9.10, is fitted by a polynomial of $\log(\sigma)$ (equation 9.11), and allow, for a given composition, extrapolation to different stresses and temperatures.

$$P = \frac{\log(t_R) - \log(t_a)}{T - T_a} \quad (9.10)$$

$$P = b_0 + b_1 \log(\sigma) + b_2 (\log(\sigma))^2 + \dots + e_i \quad (9.11)$$

where t_R is the time to rupture, T the test temperature, t_a and T_a adjustable parameters, b_i the coefficients of the polynomial and e_i an error term. As can be seen in the datasheet NRIM 28B, these parameters vary significantly even between different heats of the same grade (in this case SUS 347H, an 18Cr-12Ni-Nb wt% stainless steel).

The limitations of such methods are obvious: the composition range is limited to variation within a grade of austenitic stainless steel, or less. Non-linear effects or interactions can not be identified and extrapolations are made without any indications as to whether they are safe or not. However, they are easy to implement and to publish, consisting of a maximum of 10 parameters.

On the other hand, neural network models require substantial computational power, and printing the set of weights making up a single network is not feasible. These limitations, though, are disappearing as it is now possible to publish the software on the world wide web, as it has been done with all the models described here (www.msm.cam.ac.uk/map).

9.3 Building a database

A large database was compiled for the creep properties of various grades of austenitic stainless steels: AISI 304 (basic 18Cr-12Ni), AISI 316 (304 + Mo), AISI 321 (304 + Ti), AISI 347 (304 + Nb) and many variants designed for heat-resistant applications (for example, 316 + Ti, Esshete 1250, etc.). It contains a total of about 3500 entries which, as explained above, are equally distributed between the training and testing sets.

Figure 9.7 gives an idea of the distribution of each input against the logarithm of the rupture life. The dataset included all of the following NRIM datasheets : 5B, 6B, 45, 28A, 16B, 26B, 14B, and most of the data published by the British Steelmakers Creep Committee [112] for 304, 316, 321 and 347. Only limited data could be extracted from publications [49, 61, 113, 114, 42, 115, 26, 116, 117, 118, 119, 120, 121, 122, 123, 124]. This is essentially because of non standard pre-test mechanical treatments performed in order to accelerate the evolution of the microstructure.

The data set includes the following variables: test conditions (stress and temperature), chemical composition, solution treatment temperature and time (the latter being available in a very limited number of cases), nature of the quench following, grain size, and logarithm of rupture life. The minimum and maximum values are given in table 9.1. Be-

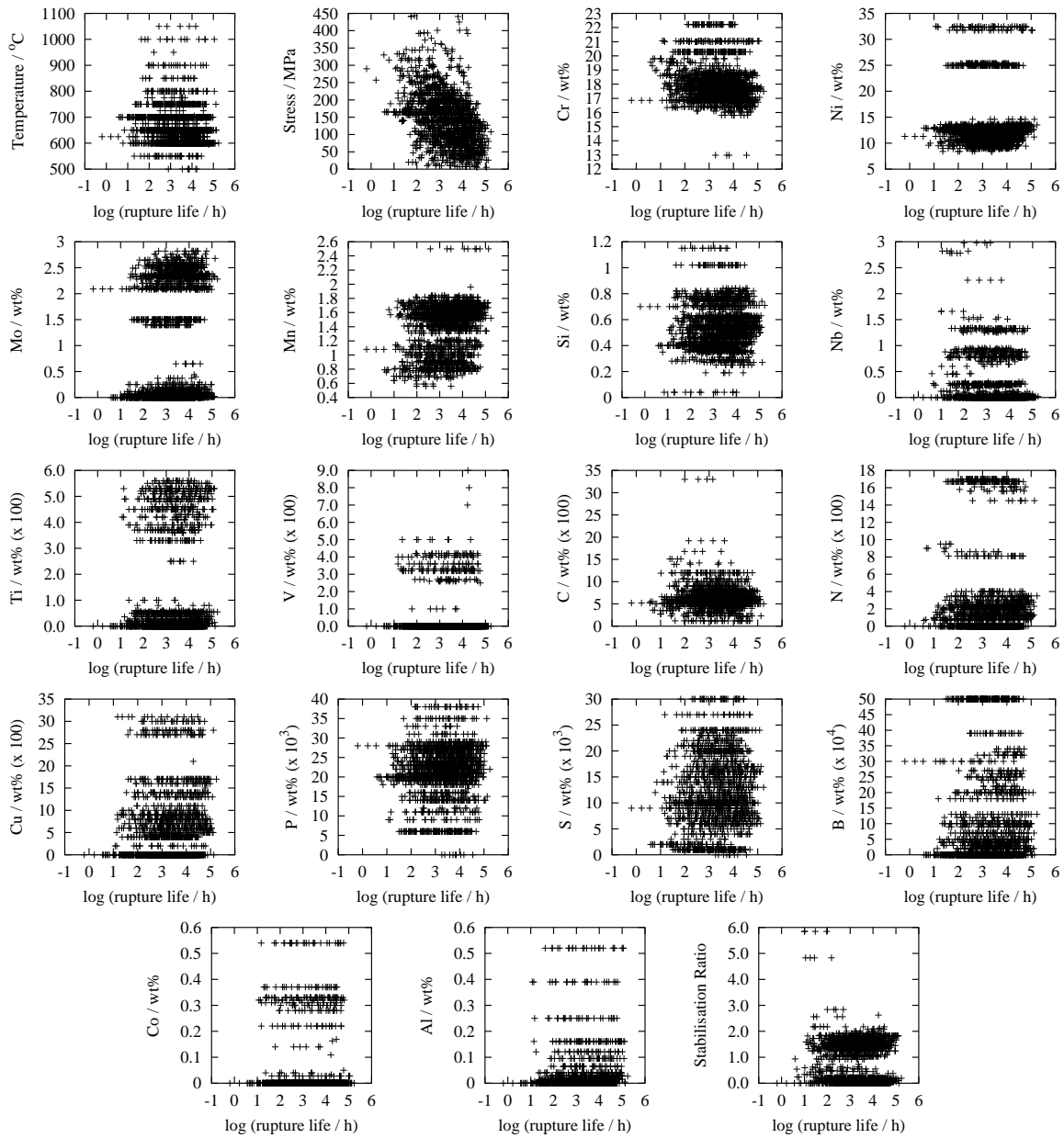


Figure 9.7: The distribution of the different inputs against the log of creep rupture life. This way of representing the data should not hide the possibility of numerous non documented interactions.

cause the algorithm includes an automatic relevance detection [110], variables which are either redundant or found to be irrelevant are affected a zero weight. There is therefore little to gain in reducing the number of input variables by any other process.

Input variable	Minimum	Maximum	Mean	Std deviation
Test Stress (MPa)	5	443	145	72
Test Temperature (°C)	500	1050	667	71
log (rupture life / h)	-0.200	5.240	3.324	0.879
Cr wt%	12.98	22.22	18.08	1.35
Ni wt%	8.40	32.48	13.82	5.47
Mo wt%	0.00	2.82	1.05	1.10
Mn wt%	0.56	2.50	1.36	0.35
Si wt%	0.040	1.150	0.545	0.171
Nb wt%	0.000	2.980	0.242	0.449
Ti wt%	0.000	0.560	0.131	0.199
V wt%	0.000	0.090	0.004	0.011
Cu wt%	0.000	0.310	0.051	0.074
N wt%	0.000	0.170	0.029	0.052
C wt%	0.012	0.330	0.062	0.025
B wt%	0.000	0.005	0.001	0.0016
P wt%	0.000	0.038	0.021	0.0067
S wt%	0.000	0.030	0.012	0.0071
Co wt%	0.000	0.540	0.037	0.1090
Al wt%	0.000	0.520	0.029	0.0804
Solution treatment temperature (°C)	1000	1350	1102	51

Table 9.1: The different inputs in the data set.

Compositional data were often missing. In such circumstances, elements usually known to be deliberate additions were set to zero while impurities were set to the average of the available data (e.g. phosphorus and sulphur). There is undoubtedly a regrettable loss of information when the amounts of elements such as Mo or Nb present as impurities are not given, as there is evidence that these elements have an influence [6].

9.4 Creep rupture life model

It is usual to attempt to predict the rupture strength for a given life time. However, the creep stress is only present as a finite number of discrete values while the rupture life is much more continuously spread, and therefore seemed a more appropriate target.

When training a model, the choice of input variables is of great importance. Also, when a combination of these variables is believed to be of particular importance, the

model can be improved by adding the combination as an explicit variable. The model was trained on the logarithm of the rupture life rather than the rupture life itself, and the calculated stabilisation ratio was used, as given below:

$$\text{Stabilisation Ratio} = \frac{\text{Nb}/8 + \text{Ti}/4}{\text{C} + \text{N}} \quad (9.12)$$

where the concentrations are in weight %. This is because precipitation of MX (where M is either Nb or Ti and X either C or N) is believed to be of particular importance to the creep behaviour of austenitic stainless steels, as will be discussed in more detail later. To avoid biasing the model, the individual variables making up the stabilisation ratio are also included, so that a direct influence of any of them can also be detected. Other input variables are as given in table 9.1.

Because some inputs were not always given (the solution treatment temperature for example), about 1000 amongst the 3500 entries of the database could not be used.

About 130 networks were trained with up to 22 hidden units and 6 different seeds. As expected, the perceived level of noise during training decreases as the model becomes more complex. The results of the training are shown in figure 9.8.

The purpose and method for building a committee model has been discussed earlier. In this case, the optimum committee was found to have 4 members. The perceived significances σ_w for these four models are shown in figure 9.9. They represent the extent to which a particular input explains the variation of the output, rather like a partial correlation coefficient in a multiple linear regression analysis.

The predictions of the final committee model (figure 9.10) contain a very few outliers considering that there is a total of about 2000 points. The improvement is clear compared with the best model alone.

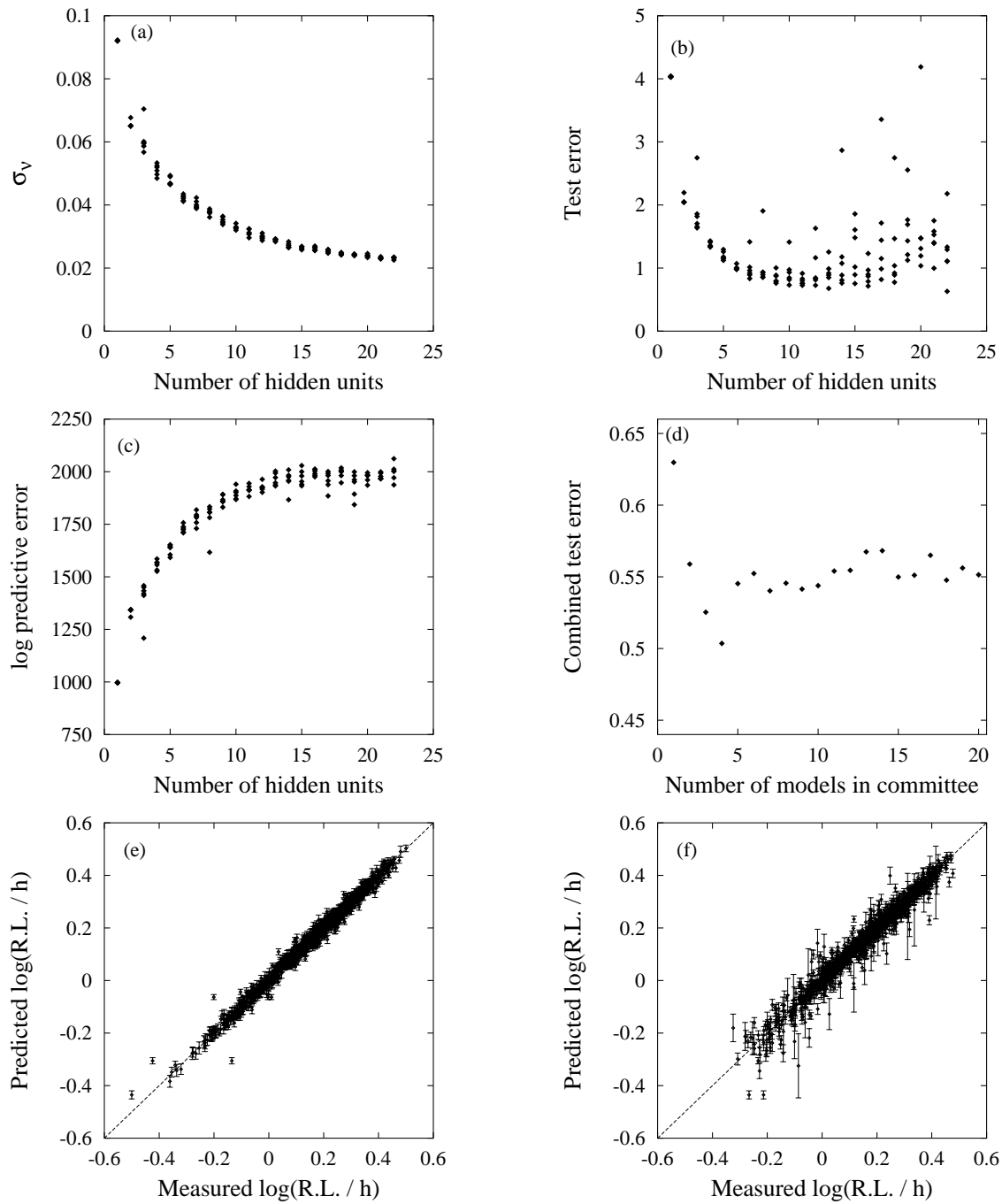


Figure 9.8: The perceived level of noise σ_v (a), the test error (b), the log predictive error (c) of the models with increasing numbers of hidden units, the combined test error (d) for an increasing number of models in committee, and the performances of the best single model on seen (training set, (e)) and unseen data (testing set (f)). (e) and (f) are plots of the predicted rupture life (R.L.) against the experimental values, in this case both are normalised.

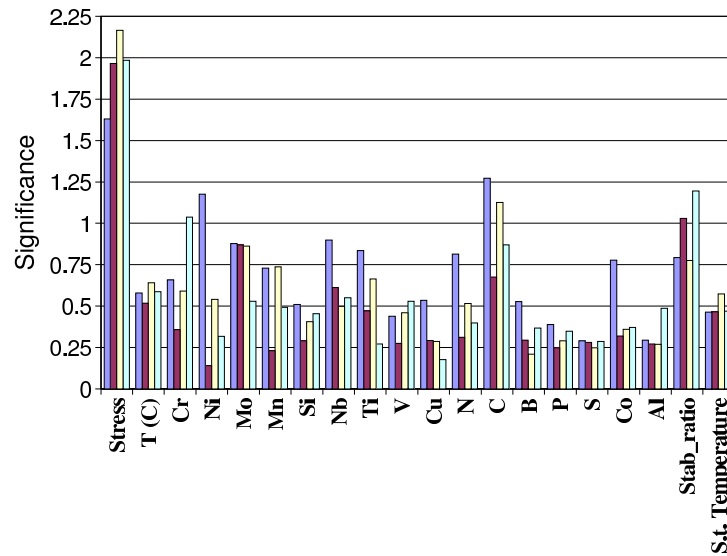


Figure 9.9: The perceived significances σ_w for the first four networks, constituting the committee model for the creep rupture life. S.t. stands for solution treatment.

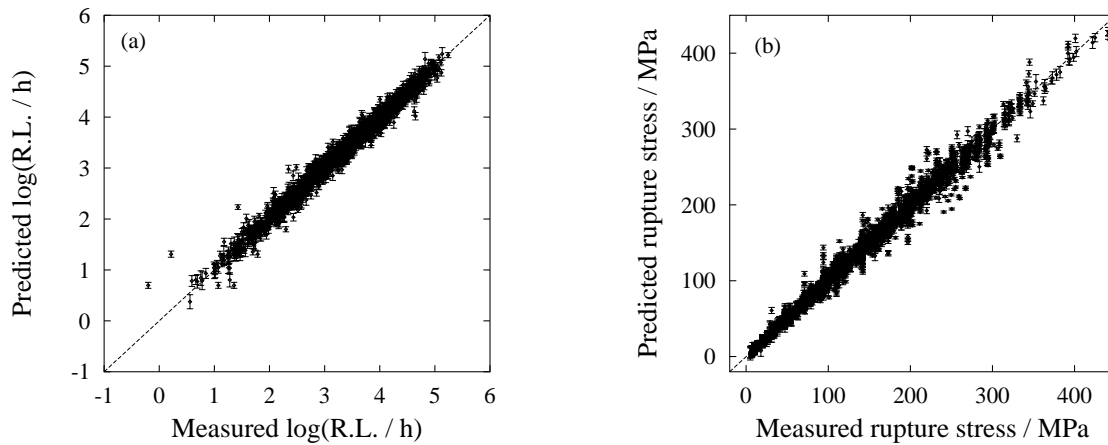


Figure 9.10: The performances of the final committee model on the whole database, for the rupture life model (a) and the creep strength model (b).

9.5 Creep strength model

The creep strength model was built essentially to facilitate quantitative comparisons with literature. In this case, the target was the stress and the life time was an input. The solution treatment temperature was not included to allow use of the entire database.

It seems of little interest to reproduce here all the results from the training such as test error or LPE as a function of number of hidden units as their evolution was similar to that observed for the creep rupture life model. In this case, the optimum number of models in committee was found to be 12. The performance of the committee is shown in figure 9.10.

9.6 Applications

9.6.a Molybdenum in AISI 304 and AISI 316

The difference between AISI grades 304 and 316 resides essentially in the addition of about 2 wt% of molybdenum. The chromium and nickel concentrations are smaller and larger, respectively, for AISI 316 compared to AISI 304. Rupture stresses for 10^4 h at 650 °C are respectively around 80 MPa and 110 MPa [125].

There are no specifications as to what the maximum level of molybdenum should be for the AISI 304 steels. It is common to find up to 0.5 wt% Mo in these steels. For AISI 316, an addition of 2-3 wt% Mo is specified. It has been shown that molybdenum has a beneficial effect on creep strength because of its solution strengthening role, although this effect can disappear after prolonged ageing due to the formation of Mo-rich Laves phase [6].

Figure 9.11 illustrates the predicted effect of molybdenum on the 10^4 h rupture stress. The initial increase is consistent with equation 9.9, which predicts a strong effect of small additions of Mo in 304. The predicted gradient (assuming a linear variation) is 38 MPa / wt% between 0 and 0.02 Mo wt%, which is lower than the one given by equation 9.9. Particularly interesting is that the trend between 0 and 1.1 wt% of molybdenum shows an excellent agreement (correlation 0.995) with a $c^{1/2}$ (where c is the concentration) dependence expected for a solution strengthening mechanism [126].

The flattening of the curve would be consistent with precipitation of a molybdenum

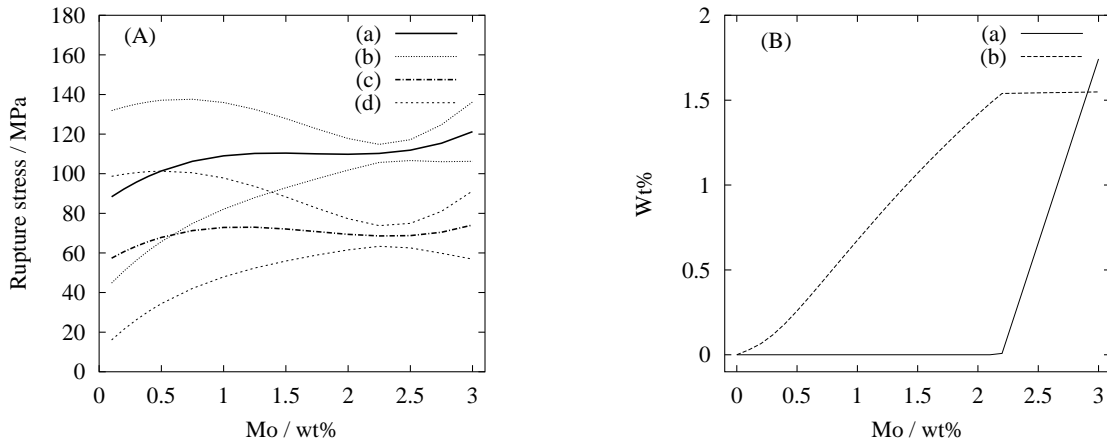


Figure 9.11: (A) The predicted effect of Mo on (a) the 10^4 h and (c) the 10^5 h rupture stress at $650\text{ }^\circ\text{C}$, (b) and (d) are the error bounds for (a) and (c) respectively. (B) MT-DATA prediction for (a) the amount of Laves phase and (b) the amount of Mo in solid solution in austenite for a steel of same composition (phases allowed were austenite, M_{23}C_6 , M_6C , Laves phase, σ phase, ferrite and liquid). The base composition used can be found in table 9.2.

rich phase, which would keep the matrix content at a constant level. In this regard, the shift of the plateau between the 10^4 h and the 10^5 h rupture stress could be related to the kinetics of this precipitation. Calculations made on this composition with MT-DATA (fig. 9.11B) actually reveal a consistent trend in the Mo content of the austenite when increasing the bulk Mo content, but indicate that Laves phase is only expected for Mo content greater than 2.2 wt%.

9.6.b Chromium and boron

According to equation 9.9, chromium slightly reduces the creep rupture strength. Unfortunately the mechanism does not seem to be understood. It was possible to reproduce this trend for a type 316 steel as illustrated in figure 9.12. The gradient for compositions close to 16 wt% Cr is in very good agreement with the value of 7.5 found in equation 9.9.

Additions of boron have been found to increase substantially the creep life of austenitic stainless steels, as emphasised by the large coefficient it is attributed in equation 9.8. The predicted effect of boron was found to be similar, with a slope of about $5700\text{ MPa} / \text{wt}\%$ (see figure 9.12).

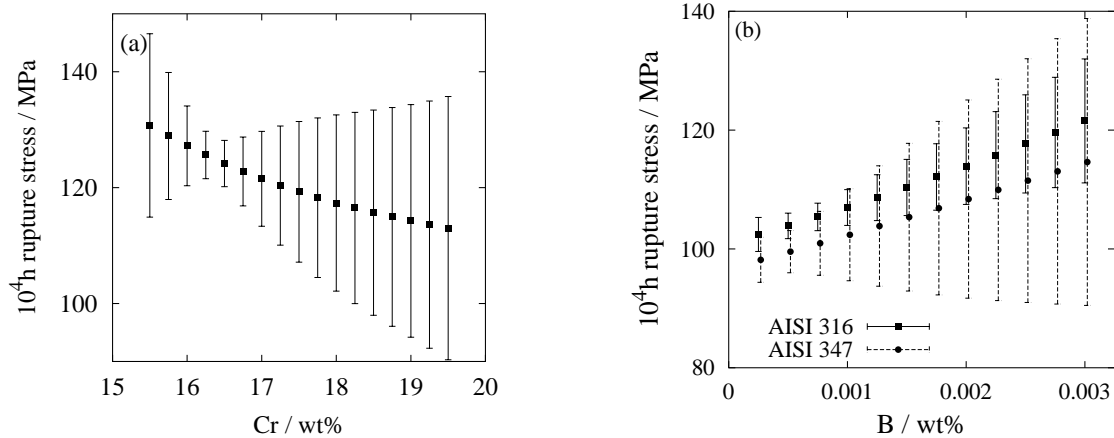


Figure 9.12: (a) The predicted influence of chromium on the 10⁴ h rupture stress at 650 °C for a typical 316. (b) The effect of boron on the creep rupture stress for two different steels. Detailed compositions for these examples are given in table 9.2

9.6.c The stabilisation ratio and solution temperature

There has been much work on the influence of the amount of ‘stabilising elements’ such as Nb, Ti, V or Zr, which prevent the formation of chromium carbides, on the creep properties of austenitic stainless steels. The problem is generally described using a stabilisation ratio (eq.9.12), which is a convenient estimate of the extent to which carbon, nitrogen and the stabilising elements deviate from stoichiometry during compound formation [12, 116, 127].

Keown and Pickering [116] estimated that the best creep properties were obtained for stoichiometric additions of Nb while more recent work [11] claims that ‘under stabilising’ C is better. This is because data from long term experiments [11] have shown that the trend observed by Keown and Pickering for rather short term experiments (average 3000 h) do not extrapolate well. For Ti on its own, the agreement is that a larger stabilisation ratio produces the optimum creep strength [6]

For short term tests, optimum creep properties have often been found when the precipitation of MX was maximised by using stabilisation equal to or greater than unity. However, according to [6], the creep of austenitic steels is essentially diffusion controlled in service conditions, which could explain why there is no great benefit in maximising the amount of MX precipitates.

Figure 9.13(a), shows that the neural network model was able to reproduce the ex-

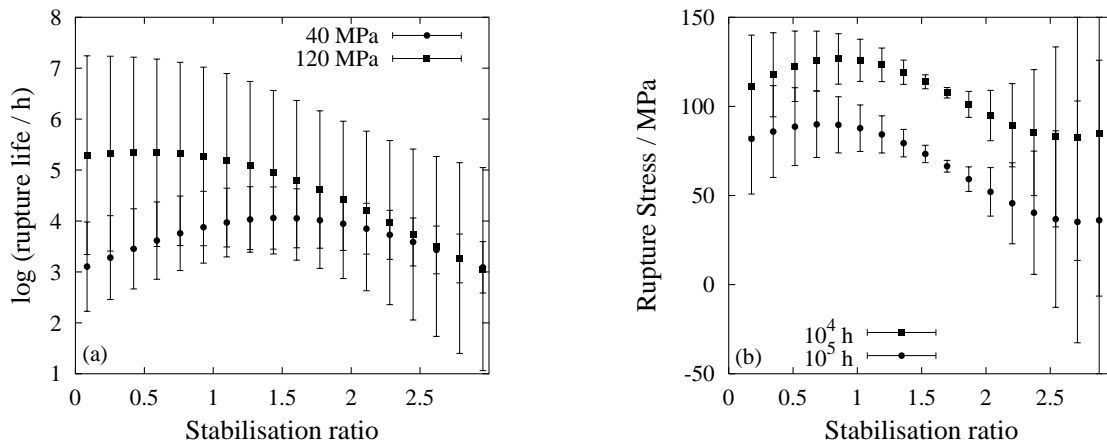


Figure 9.13: (a) The effect of the stabilisation ratio (increase of Nb) on the creep rupture life of a typical 18Cr-12Ni steel at 650 °C. Optimum short term creep properties are obtained for close to stoichiometric additions, while understabilisation is better for long term properties. (b) the effect of an increase of Ti: the stabilisation ratio which produces the optimum creep strength is larger than in (a).

pected trends for Nb additions. For short term tests, the best properties are obtained for a stabilisation ratio equal to or slightly greater than unity. For longer term tests, the influence of stabilising elements is predicted to be less and the optimum addition much below a stoichiometric ratio. On the right of the same figure is the effect of Ti addition on the 10⁴ and 10⁵ h rupture stress of a typical 18-12 steel, showing that the model correctly predicts best properties at a larger stabilisation ratio, although this ratio still shifts slightly towards understabilisation for longer times.

Figure 9.14 (a), shows the effect of the solution treatment temperature for different levels of Nb (see base composition in table 9.2). This is in very good agreement with the hypothesis [12] that the optimum creep properties are obtained when as much as possible of MX forming elements are put in solution before service: with an increased level of niobium, the solution treatment temperature that dissolves the maximum amount of Nb(C,N) is increased. Figure 9.14(b), is a prediction of the amount of NbC (calculated with MT-DATA [83]) found in a steel of composition equal to that used for the predictions above, (steel with 0.32 Nb wt%). It shows that all of the carbon and niobium are in solution only at temperatures larger than 1250 °C, which closely matches the optimum solution treatment temperature for this composition.

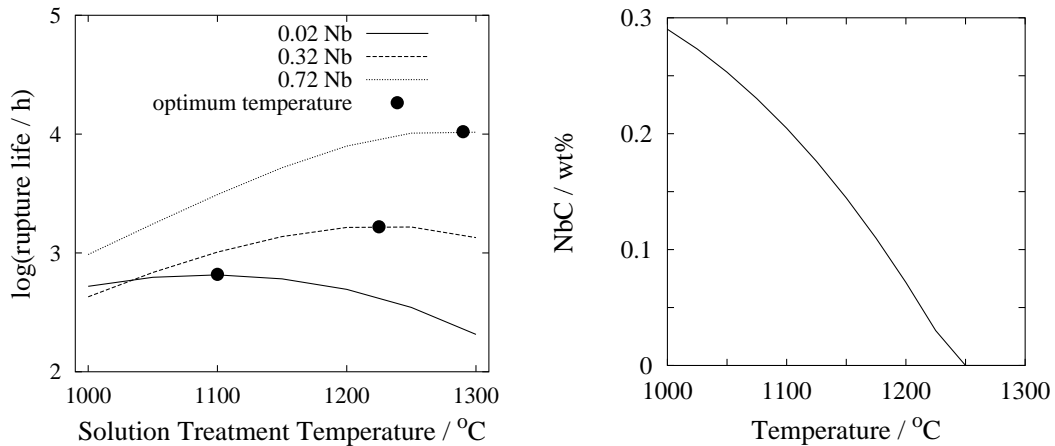


Figure 9.14: (a) the predicted effect of the solution treatment temperature on the creep rupture life of a typical 18-12 steel (see table 9.2). On the right, the amount of NbC present as a function of the solution treatment temperature, in the 0.32Nb wt%, calculated with MT-DATA (allowing for austenite, ferrite, liquid, TiC, NbC, TiN, NbN, $M_{23}C_6$ and σ -phase). The solubility limit corresponds closely to that for which optimum creep properties are predicted.

9.6.d Comparison with other methods

The recent revision of the NRI (National Research Institute for Metals, Japan) datasheet no. 28 (28B, data for SUS 347H TB) contains considerably more long term data than did the previous version 28A. At the time when the database used in the present work was compiled, these new data were not available and therefore have not been used to train the models. It is interesting to compare the predictions of our model with those made by the NRI on the same data.

The 10^5 h rupture stress was predicted using the neural network model for two steels of the NRI 28B datasheet (AEA and AEG), for temperatures ranging between 600 and 750 °C.

Figure 9.15 shows the predictions of the neural network model against those made by the NRI, using the Orr-Sherby-Dorn method, on the previously published data, and the recent results published in revision 28B. The agreement with experimental data is good, particularly in the case of steel AEG where the neural network produces significantly better predictions than the Orr-Sherby-Dorn method used by the NRI. It should also be noticed that the trends for both steels have been correctly predicted, despite their apparent similarity in composition (see table 9.2).

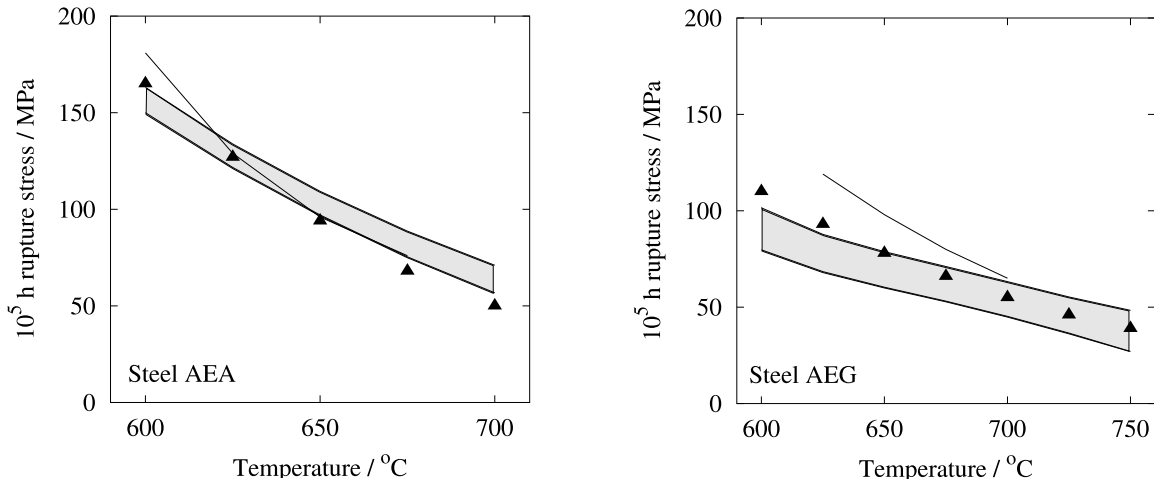


Figure 9.15: Comparison between the neural network model predictions (shaded area), the predictions made by NRRM using the Orr-Sherby-Dorn method (line) and the experimental values published in the recent revision 28B (points). See table 9.2 for full compositions.

9.6.e Software

A number of other trends predicted by the models have been examined, which have been found to be reasonable from a metallurgical point of view, amongst which a positive effect of Cu, of P within a limited range (however this element causes embrittlement and is therefore kept much below the level giving optimum creep rupture strength). The number of possibilities of interactions are such that it is not possible to study them fully. The database used to create the model covers a large range of compositions and its application does not stop at the AISI 300 series. The software capable of doing these calculations can be obtained freely from <http://www.msm.cam.ac.uk/map/map.html>.

9.7 Summary and conclusions

The creep rupture life for a given stress, and the creep rupture stress for a given life have been analysed using a neural networks method within a Bayesian framework. The data were obtained from a variety of sources and cover a wide range of compositions and heat treatments. The potential of the method is clearly illustrated in its ability to perceive interactions between the different input variables. Predicted trends have been found consistent with those expected and the quantitative agreement was frequently

Fig.	Cr	Ni	Mo	Mn	Si	Nb	Ti	V	Cu
9.11	18.0	12.0	-	1.4	0.6	0	0	0	0
9.12(a)	-	12.1	2.54	1.41	0.46	0	0	0	0
9.12(b) 316	16.42	13.21	2.34	1.51	0.52	0.01	0.011	0	0.14
9.12(b) 347	17.89	12.55	0.11	1.74	0.77	0.77	0.02	0.033	0.09
9.13(a)	18.15	13.3	0	0.75	0.4	0.1	0	0	0
9.13(b)	17.71	12.27	0.02	1.56	0.55	0.005	-	0	0.06
9.14(a)	18	12	0.05	0.8	0.4	0.02	0.02	0	0
9.15(AEA)	17.85	12	0.04	1.71	0.60	0.74	0.019	0.031	0.05
9.15(AEG)	17.56	12.24	0.15	1.81	0.63	0.87	0.019	0.041	0.14
Fig.	N	C	B ppm	P	S	Co	Al		
9.11	0	0.06	5	0.02	0.01	0	0		
9.12(a)	0	0.04	0.0002	0.019	0.02	0	0		
9.12(b) 316	0.034	0.05	-	0.021	0.01	0	0		
9.12(b) 347	0.016	0.05	-	0.025	0.007	0.37	0.004		
9.13(a)	0.012	0.062	0	0.02	0.002	0	0		
9.13(b)	0.014	0.06	5	0.026	0.01	0	0.121		
9.14(a)	0.01	0.06	10	0.02	0.002	0	0		
9.15(AEA)	0.0284	0.07	12	0.02	0.005	0.29	0.019		
9.15(AEG)	0.0222	0.053	27	0.027	0.011	0.30	0.008		

Table 9.2: The base compositions of the different examples, in wt%.

satisfying. The model can be applied widely because of its capacity to indicate uncertainty, including both an estimate of the perceived level of noise in the output, and an uncertainty associated with fitting the function in the local region of input space.